energies

MDPI

Article

Layout Design and Network Modeling of Linear PV Power Plant with MVDC Architecture

Baoling Guo *, Melaku Adhana, Didier Blatter, Julien Pouget and Brice Beuchat

School of Engineering, University of Applied Sciences and Arts of Western Switzerland, 1950 Sion, Valais, Switzerland; didier.blatter@hevs.ch (D.B.); julien.pouget@hevs.ch (J.P.)
* Correspondence: baoling.guo@hevs.ch

Abstract

Energy Strategy 2050 promotes photovoltaic (PV) deployment to reduce fossil fuel dependence in Switzerland. However, limited available land constrains conventional solar farms, motivating the deployment of linear PV (LPV) systems along transport corridors such as highways or railways. This paper contributes to a systematic design and modeling methodology for an LPV power plant interconnected through a medium-voltage direct current (MVDC) collection network. The main methodological contribution is the development of a modified iterative modified nodal analysis (MNA) framework tailored to LPV–MVDC systems. In long-distance feeders with high line impedance, nonlinear voltage–current coupling becomes significant. These nonlinearities cannot be accurately captured by conventional MNA assuming fixed current injections. The proposed iterative approach can more accurately capture these effects compared to conventional MNA. A case study of a 5 km railway-based LPV system is investigated to present the design and modeling methodology, including layout design, network modeling, and cable sizing. The LPV power plant reaches a peak power of 3.4 MW and requires 40 DC/DC converter stations rated at 100 kW each. Cable analysis shows that 6 mm^2 copper conductors satisfy voltage drop limits at a string level, while 95 mm^2 conductors maintain MVDC voltage variations within 3%. These results highlight technical feasibility of MVDC-based integration for efficient long-distance renewable energy distribution.

Keywords: linear PV; railway network; DC/DC converter; multi-MPPT; MVDC network; layout design; modified nodal analysis

1. Introduction

Energy Strategy for 2050 aims to reduce the country's dependency on fossil fuels in Switzerland, by developing renewable energy supply, with a particular focus on photovoltaic (PV) [1]. However, the country's mountainous terrain, extensive agricultural and settlement areas, and high land costs limit the availability of large open spaces for conventional solar farms, necessitating innovative deployment approaches [2]. Several studies have explored linear photovoltaic (LPV) systems and vertical solar panel configurations as promising solutions for narrow and elongated areas such as highways, pipelines and railway corridors [2–5]. The potential for large-scale deployment of vertical solar panels along Europe's major roads and railways has been assessed in [6]. This work indicates that the integration of PV systems into transport infrastructure could make a substantial contribution to the energy transition.

Check for updates

Received: 2 June 2026
Revised: 26 June 2026
Accepted: 3 July 2026
Published: 8 July 2026

Copyright: © 2026 by the authors. Licensee MDPI, Basel, Switzerland. This article is an open access article distributed under the terms and conditions of the Creative Commons Attribution (CC BY) license.

However, the extended physical layout of LPV plants and the considerable distance between the PV installations and the available AC grid substation present challenges for the distribution networks [7,8]. As a result, challenges such as large voltage variations, increased power losses, and reduced network stability may arise. Traditional medium-voltage alternative current (MVAC) collection networks suffer from higher power losses and notable voltage drops over long distances [7]. These limitations have motivated the exploration of alternative solutions, among which medium-voltage direct current (MVDC) technology has emerged as a promising option. MVDC technology is emerging in power distribution systems following the expansion of the high voltage direct current (HVDC) in power transmission [8–11]. Recent research has demonstrated the growing interest in MVDC architectures in modern distribution systems [12–14]. The main advantages of MVDC solutions are analyzed in terms of energy efficiency, power dispatch, power capacity, raw material consumption, CO_2 emissions and distribution network resilience in [15]. Furthermore, the potential of MVDC systems for renewable energy integration has been investigated in both photovoltaic and wind power applications [16,17]. Since 2023, the OPHELIA pilot project has been developing a demonstrator of an LPV power plant based on an MVDC collection network [18]. MVDC networks can overcome limitations present in AC transmission, such as reactive power losses and skin effect, thereby reducing line losses and improving overall system efficiency. MVDC architectures also facilitate the flexible integration of renewable energy sources and battery energy storage systems into renewable-energy-based microgrids [2]. The LPV power plant interconnected with an MVDC collection network is therefore considered in this work, given its potential to provide a reliable and efficient solution for long-distance power distribution.

The core components of an LPV power plant using an MVDC collection network are the DC/DC converters that connect PV arrays to the MVDC networks. Both research and industry pay increasing attention to high-ratio, high-power converter technologies for such applications. These DC/DC converters, often referred to as DC solid-state transformer (DC-SST) or isolated high-voltage DC/DC converter, combine high-frequency switching, medium-frequency transformer, and Silicon Carbide (SiC) semiconductor devices to achieve high efficiency, compact design, and galvanic isolation [19]. One relatively mature solution is the DC-SST developed by the SuperGrid Institute, offering a 1.2 kV to ±10 kV (20 kV) isolated DC/DC conversion at 250 kW [19]. Each DC/DC converter station includes multiple boost converters for MPPT. The prototype has been implemented in a demonstrator project [18]. Aalborg University and ETH Zürich have respectively developed MV DC/DC converters using 10 kV SiC devices and medium-frequency transformers, though typically at lower power levels around 10 kW [20,21]. Commercial solid-state transformers from companies such as RCT Systems operate at comparable voltage classes but are generally AC-to-DC or MV-to-LV devices and therefore not directly suitable for MVDC distribution integration [22]. Regarding the MVDC-to-AC grid interface, megawatt-level AC/DC converters are commercially available and widely deployed in MVDC or HVDC applications. These systems are primarily based on a voltage source converter (VSC), commonly using a three-level converter and modular multilevel converter (MMC) [23,24]. MMCs can be scaled to very high voltages using low-voltage sub-modules. Their low switching losses ensure high efficiency at large power levels. These characteristics make MMCs suited for high-power and high-voltage MVDC applications. This work focuses on the modeling and sizing of LVDC/MVDC networks. A detailed modeling and control of the DC-to-AC grid interface are beyond the scope of this study. Overall, most DC/DC converter technologies remain at the research or prototype stage; no commercial products are currently available on the market. In this work, the DC-SST with multiple boost converters for MPPT used in [19] is considered, as the multiple MPPT channels help mitigate module mismatch issues

that arise in long-distance LPV installations. It is worth noting that, as there are currently no commercial converter products available, the design presented in this work provides only theoretical results regarding PV array size and converter capacity. However, the modeling and sizing methodologies can be flexibly replicated to match the actual specifications of the converters used in a real project.

The LPV design must account for challenges imposed by both electrical standards and land constraints associated with highways or railway corridors. LPV installations exhibit narrow and elongated layouts imposed by the available corridor geometry, causing their layout and arrangement to differ from that of conventional PV plants. The extended length results in spatially varying solar irradiance conditions along the LPV plant. Consequently, a trade-off exists between PV module mismatch losses and the number of modules connected per string [5]. In addition, the electric collection network configurations must comply with voltage constraints along collection cables and feeder lines, in accordance with PV installation guidelines [25]. Voltage rise along the feeder line between the MVDC bus and the LPV plant connection point can be approximated as linear. However, voltage variations along MVDC collection cables present nonlinear behavior due to the distributed nature of PV power injection along the MVDC network. Consequently, a modeling approach capable of simultaneously capturing both linear and nonlinear voltage variations is required. However, systematic design methodologies that include both detailed LPV layout design and electrical network modeling remain limited in the literature. The break-even distance, power losses, and total costs have been calculated and compared between AC and DC collection networks in [7,15], but these studies do not specifically address LPV systems. Another work proposed a layout optimization method for LPV arrays on railway embankment slopes [5], yet the collection network was not involved. A recent study investigated the design of a 20 MW LPV-MVDC system extending over 20 km [8]. However, the network modeling approach was not described in detail. The layout design for a vertically oriented LPV system was not comprehensively addressed either. To the best of the authors' knowledge, existing literature lacks a systematic design and modeling framework for LPV systems interconnected through an MVDC network along long-distance transport corridors. In particular, a unified approach that simultaneously addresses detailed layout design, complex network modeling, and cable sizing is still missing. This gap constitutes the primary motivation of the present work. Furthermore, the main methodological challenge lies in the modeling of an MVDC network integrating distributed converter-interfaced PV generation. The modified nodal Analysis (MNA) is a systematic circuit analysis method widely used to formulate DC network equations [26,27]. It enables efficient computation of node voltages and branch currents in complex electrical circuits. Conventional DC power-flow methods generally rely on bus–branch representations and decouple network equations from the circuit structure [28,29]. In contrast, MNA preserves the physical network structure through circuit-based formulation and enables explicit representation of electrical components. This allows a flexible modeling of feeder impedance, multiple voltage sources, distributed PV current injections, and potential distributed loads (e.g., moving trains) within a single matrix framework. Therefore, it provides a more flexible and scalable formulation for large-scale LPV-MVDC systems. However, LPV systems connected through MVDC networks exhibit characteristics that can not be fully captured by conventional MNA formulations.

The reasons are explained as follows. In a standard MNA, distributed PV arrays are typically modeled as current sources. However, converter-interfaced PV arrays operating under MPPT control behave more closely as constant-power sources. Consequently, the injected current at nodes depends on the local node voltage. Meanwhile, the node voltages vary along the MVDC network due to line impedance and distributed PV current injections. This voltage–current coupling introduces nonlinearities that cannot be accurately captured

by conventional MNA assuming fixed current injections. To address this issue, a modified MNA framework with an iterative solution scheme is proposed. The iteration helps consistently update voltage-dependent PV current injections at each node. The methodological novelty does not lie in the iterative procedure itself but in the development of a modified MNA framework specially adapted to LPV systems interconnected by an MVDC network. The iterative scheme ensures accurate representation of nonlinear voltage–current coupling while maintaining the flexibility and scalability of the MNA framework.

1.1. Research Gap

Despite the significant potential of LPV solutions along transport corridors, the aforementioned discussion highlights that several research gaps remain, as summarized below:

- First, existing literature lacks a systematic design and modeling framework for LPV systems connected with MVDC networks along long-distance transport corridors. Particularly, one that simultaneously addresses detailed layout design, complex network modeling, and cable sizing.
- Second, the main methodological challenge lies in the modeling of MVDC networks integrating distributed converter-interfaced PV generations. The conventional MNA approach exhibits limited modeling accuracy when applied to LPV-MVDC systems. An enhanced MNA formulation is required to enable accurate and efficient modeling of large-scale long-distance LPV networks.
- Finally, systematic design guidelines tailored to LPV with MVDC architectures remain limited in the literature, particularly for railway- and highway-based deployment scenarios. In these contexts, spatial constraints and electrical design principles must be addressed jointly, as both factors influence overall system performance.

1.2. Contributions and Innovations

To address the aforementioned gaps, this paper contributes a systematic design and modeling framework for LPV power plants connected via MVDC architecture. The key methodological novelty is the development of an iterative MNA framework specially adapted to LPV-MVDC systems. The contributions are specified as follows:

- A systematic layout design is presented for a vertical LPV power plant that considers both spatial installation limitations and electrical safety constraints.
- A dual-layer electrical modeling framework is developed to decouple the PV string LVDC network from the MVDC collection network. The proposed method can capture both PV local behaviors at the LVDC level and voltage variations induced by long-distance power transfer along an MVDC network.
- A modified MNA approach incorporating an iterative solution is proposed to address the resulting nonlinearities along the MVDC network. The iterative scheme effectively captures the voltage-dependent behavior of converter-interfaced PV generation. This enables accurate evaluation of nonlinear voltage profiles in long-distance LPV systems while preserving the flexibility and scalability of the MNA framework.
- A case study of a 5 km LPV railway corridor is investigated to demonstrate the applicability of the proposed methodology. In addition, it provides engineering design guidelines for converter sizing, cable selection, and system configuration.

The remainder of this paper is organized as follows: Section 2 describes the layout design for the LPV power plant. Section 3 presents the detailed modeling approach for the PV string circuit and the proposed iterative MNA method for analyzing the MVDC network with distributed PV generation. Section 4 discusses the results and provides cable sizing guidelines for both LVDC and MVDC levels. Section 5 provides a brief discussion on

study limitations, practical challenges and expected economic impacts. Section 6 concludes key results and outlines future work.

2. Layout Design and Sizing of LPV Power Plant

The case study is assumed to deploy PV modules arranged in a two-row linear vertical configuration extending along a 5 km railway corridor, as presented in Figure 1. Each PV arrays installed along two sides are controlled by one DC/DC converter. The distance between PV panels is set to $L_d = 0.1$ m. The distance reserved for DC/DC converter installation is set to $L_D = 1.5$ m. In addition, the Meyer Burger PV module is selected for this study, and its key specifications are provided in Table 1. It is noted that these parameters provided in Table 1 correspond to standard test conditions (STCs), defined as an irradiance of 1000 W/m^2 and a module temperature of 25 °C. The layout design of the PV string and array, as well as their sizing, will be detailed in the following sections.

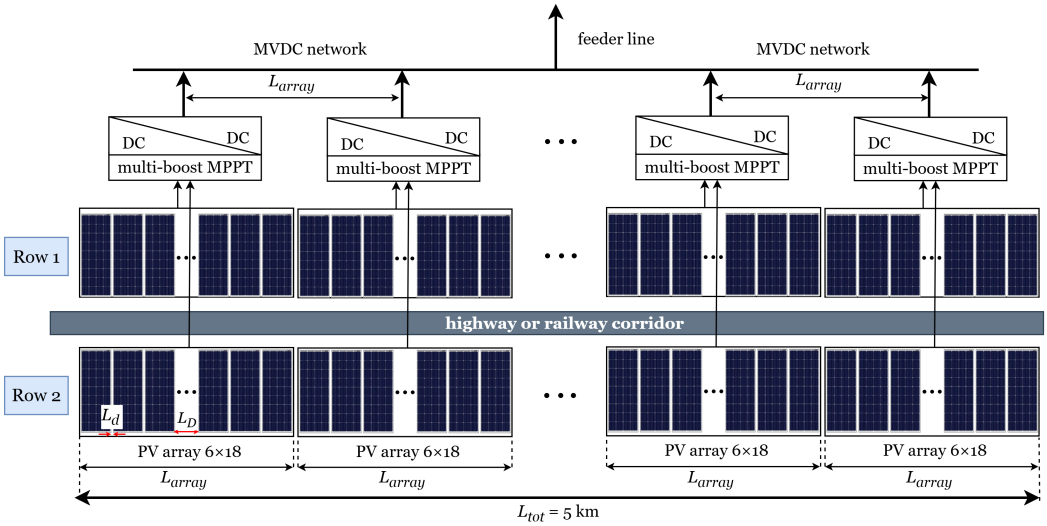


Figure 1. Physical layout design of two-row linear vertical PV power plant.

Table 1. PV module specifications, data compiled from the technical datasheet of Meyer Burger Technology AG [30].

Parameter	Value
Module power	395 W
Module efficiency	21.5%
Module length	1.767 m
Module width	1.041 m
Voltage at MPP V_{MPP}	39.2 V
Current at MPP I_{MPP}	10.1 A
Open-circuit voltage V_{oc}	44.7 V
Short-circuit current I_{sc}	10.6 A
Maximum system voltage	1000 V
Temperature coefficient $\alpha_{I_{sc}}$ for I_{sc}	+0.033%
Temperature coefficient $\beta_{V_{oc}}$ for V_{oc}	−0.234%
Nominal module operating temperature	44 ± 2 °C

2.1. Layout and Sizing of LPV String

The maximum system voltage, corresponding to the maximum open-circuit voltage of the PV system, must be respected to ensure safety, avoid equipment failure, and maintain compliant and reliable installation with electrical standards. The PV voltage during production is less than the maximum system voltage. When designing a LPV string, it is essential to consider the manufacturer's specified maximum system voltage provided in Table 1 and the impact of temperature fluctuations on PV module voltage. Rising temperatures lower the PV voltage and slightly increase the current, whereas falling temperatures cause a significant increase in voltage. This voltage increase at low temperatures can exceed system voltage limits, making precise voltage calculations necessary to ensure safe and efficient operation. The effect of temperature on the output voltage and current of a PV module is calculated over different temperature ranges using equations as follows [31]:

$$V_{oc}(T) = V_{oc} \times (1 + \beta_{V_{oc}}(T - 25)) \tag{1}$$

$$I_{sc}(T) = I_{sc} \times (1 + \alpha_{I_{sc}}(T - 25)) \tag{2}$$

where T [°C] is the module operating temperature, $V_{oc}(T)$ [V] is the open-circuit voltage at temperature T, $I_{sc}(T)$ [A] is the short-circuit current at temperature T, $\alpha_{I_{sc}}$ [%/°C] is the temperature coefficient for current, and $\beta_{V_{oc}}$ [%/°C] is the temperature coefficient for voltage. It is noted that the value of the coefficient $\alpha_{I_{sc}}$ is quite small; the short-circuit current I_{sc} increases very slightly with the temperature. Compared to the significant effect of temperature on voltage, this change is minimal and can therefore be neglected.

The PV modules are connected in series in a string. The string voltage $V_{str}(T)$ is calculated by (3). The results with respect to different numbers of PV modules in a string $N_{M_{str}}$ of 18, 20, 22 across various temperatures are summarized in Table 2. A string of 18 modules is therefore chosen to ensure the system voltage remains within the 1000 V limit, leaving a safe margin for increased voltages at low temperatures.

$$V_{str}(T) = V_{oc}(T) \times N_{M_{str}} \tag{3}$$

with $N_{M_{str}}$ the number of PV modules connected in series in a string.

Table 2. System output voltage of a PV string at different temperatures.

Temperature [°C]	40	30	20	10	0	−10	−20	−30	−40
Voltage of 18 modules [V]	776	797	812	828	835	869	884	909	927
Voltage of 20 modules [V]	862	885	903	920	937	966	982	1010	1030
Voltage of 22 modules [V]	948	974	993	1012	1031	1063	1080	1111	1133

Each MPPT boost unit controls two PV strings installed on opposite sides of the railway corridor. The string length serves as a key indicator for evaluating power mismatch. The length of a string L_{str} is calculated by

$$L_{str} = N_{M_{str}} \times L_{mod} + (N_{M_{str}} - 1) \times L_d \tag{4}$$

with L_{mod} the PV module width and L_d the distance between adjacent PV modules.

If each string contains one line of 18 PV modules connected in series, the length of a string will be around 20.4 m. If each string is instead configured as two parallel lines of 18 modules, the total number of modules per string increases to 36, resulting in an extended string length of 40.8 m. MPPT efficiency may be adversely affected due to increased power mismatch over the longer distance. Therefore, extended string lengths may be considered

under favorable environmental conditions, such as uniform irradiance and the absence of shading from trees or other obstacles. However, in environments with potential shading or non-uniform irradiance, a moderate string length is preferable to preserve MPPT efficiency. Some previous studies have deployed optimization algorithms for LPV layout design to mitigate mismatch power losses, such as shadow-adaptive genetic algorithms, mixed-integer quadratic programming, and artificial intelligence methods [5,32,33]. However, a detailed investigation of optimization techniques is beyond the scope of this work.

2.2. Layout and Sizing of LPV Array

The array size largely depends on the DC/DC converter architecture. The DC-SST station with six multiple boost converters for MPPT used in [19] is considered in this work. Multiple MPPT channels help mitigate module mismatch issues that can arise in long-distance LPV installations. Each array comprises 6 PV strings, corresponding to the number of boost MPPT inputs. The total number of PV modules per array is calculated by

$$N_{M_{array}} = N_{M_{str}} \times N_{str} \tag{5}$$

with N_{str} the number of strings in an array. The length of each array L_{array} is calculated by

$$L_{array} = N_{M_{array}} \times L_{mod} + (N_{M_{array}} - 1) \times L_d + L_D \tag{6}$$

Each two PV arrays installed along two sides are interfaced by one DC/DC converter. Consequently, the total number of required DC/DC converters is calculated by

$$N_{DC/DC} = \frac{L_{tot}}{L_{array}} \tag{7}$$

with the following configurations: $L_{tot} = 5$ km, $L_{mod} = 1.041$ m, $L_d = 0.1$ m, $L_D = 1.5$ m, thus, $L_{str} = 20.4$ m and $L_{array} = 124.6$ m. The following results are obtained: the number of PV arrays in total is $N_{array} = 80$ and the number of DC/DC converters needed is $N_{DC/DC} = 40$. The total number of PV modules is therefore $18 \times 6 \times 2 \times 40 = 8640$. With the peak power of each PV panel $P_{mod} = 395$ W, the PV power controlled by each DC/DC converter is therefore $18 \times 6 \times 2 \times 395 = 85$ kW at MPP mode and STC condition. Each DC/DC converter is configured with a rated power of 100 kW, providing an adequate safety margin. The peak power of the LPV power plant is approximately $8640 \times 395 = 3.4$ MW. If each string is instead composed of two parallel lines of 18 modules, the number of PV modules per boost MPPT input is doubled. In this case, the number of DC/DC converters is reduced to 20 by sacrificing the MPPT efficiency due to increased power mismatch over a longer distance as explained in Section 2.1, and the rated power of the DC/DC converter is increased to 200 kW. The layout design and sizing results are summarized in Table 3.

Table 3. Configured parameters of LPV power plant.

Parameter	Case 1: Series	Case 2: Parallel | Series
Number of modules in a string	18	2×18
Length of a string	20.4 m	40.8 m
Number of strings in an array	6	6
Number of arrays	80	40
Number of total PV modules	8640	8640
Number of DC/DC converters	40	20
Rated power of DC/DC converter	100	200
Total power of LPV power plant	3.4 MW	3.4 MW

Once the LPV plant size and layout are defined, another key question arises regarding an appropriate configuration of network architecture and connection cables to ensure efficient long-distance power distribution. The following studies will focus on Case 1.

3. Modeling of LPV Collection Network

The general electrical architecture of an LPV power plant connected via a MVDC network is illustrated in Figure 2. The system design is described from both the architectural and control perspectives as follows:

- Regarding the architecture design, firstly, an MPPT boost converter is installed at the midpoint of a PV array, with six PV strings symmetrically arranged on both sides. Secondly, the PV arrays interfaced via DC/DC converters are symmetrically distributed along the MVDC network. The grid connection point is located at the center of the LPV system. Finally, the distance between the LPV power plant and the available substation for the LPV integration corresponds to the feeder line length L_f.
- Regarding the control design, firstly, the boost MPPTs regulate the output voltage at PV buses to ensure maximum power extraction of each PV string. Secondly, the isolated DC/DC converter maintains a stable LVDC bus voltage $V_{in-LVDC}$ despite power disturbances generated by the MPPT converters and voltage variations along the MVDC network. The voltage $V_{in-LVDC}$ is set to 1 kV, being larger than the maximum open-circuit voltage mentioned in Section 2.1. Finally, the MVDC bus voltage $V_{in-MVDC}$ is regulated by the AC/DC converter station connected to the AC grid. The outer voltage control loop ensures power balance between the MVDC network and the AC grid by providing the reference for the inner current control loop. The inner loop regulates the converter currents, thereby controlling the active power exchanged with the AC grid to maintain the MVDC voltage at its setpoint. The reactive power exchange can be independently controlled or adjusted according to grid-code requirements.

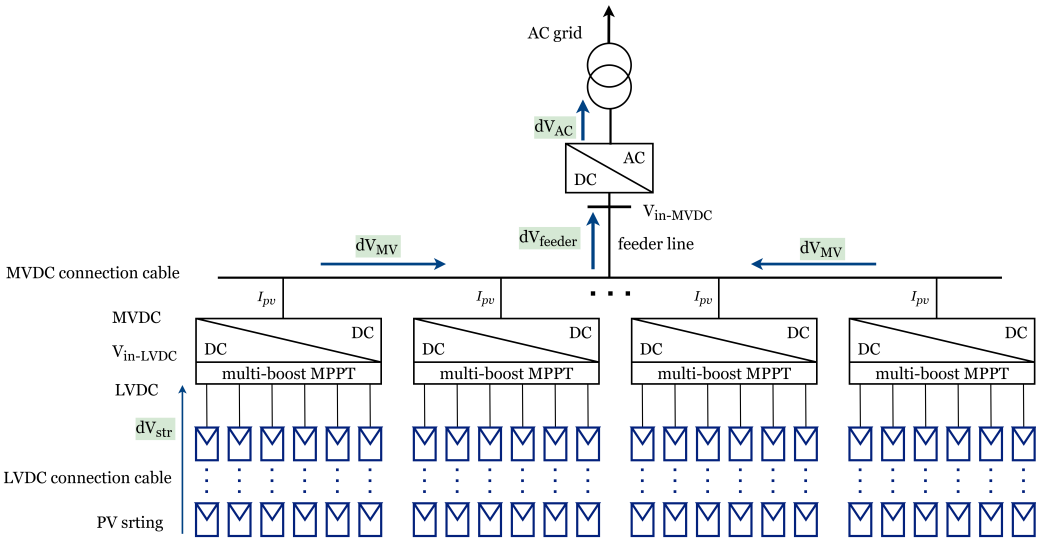


Figure 2. Global architecture design of LPV power plant using MVDC collection network.

The PV strings are regulated by boost MPPT converters and integrated into the LVDC network. The PV arrays interfaced by LV-to-MV DC/DC converters are distributed along the MVDC network. Since the LV and MV subsystems are galvanically isolated by the DC/DC converters, they are therefore modeled separately in the following subsections.

3.1. Modeling of LVDC PV String Collection Network

PV panels are connected in series and extended over a certain distance before being connected to the MPPT boost converters, as illustrated in Figure 3. The cable system includes the interconnection cables between PV panels, as well as the feeder line between the PV string and the MPPT boost converter. For large-scale installations, the cables connecting PV panels can be specified by the manufacturers according to the physical layout design (e.g., vertical or horizontal configurations). For simplicity, it is assumed that the total length of the panel interconnection cables equals the PV string length L_{str}. Accordingly, the one-way feeder length for the most remote array is equal to half of the PV array length $0.5 \times L_{array}$. In addition, since the DC/DC converter station is installed on one side of the railway track, the string located on the opposite side requires a cable crossing the track, either overhead or underground. A connection length $L_c = 5$ m is assumed here. This value may vary in practical installations and should be checked and validated during the real construction design phase.

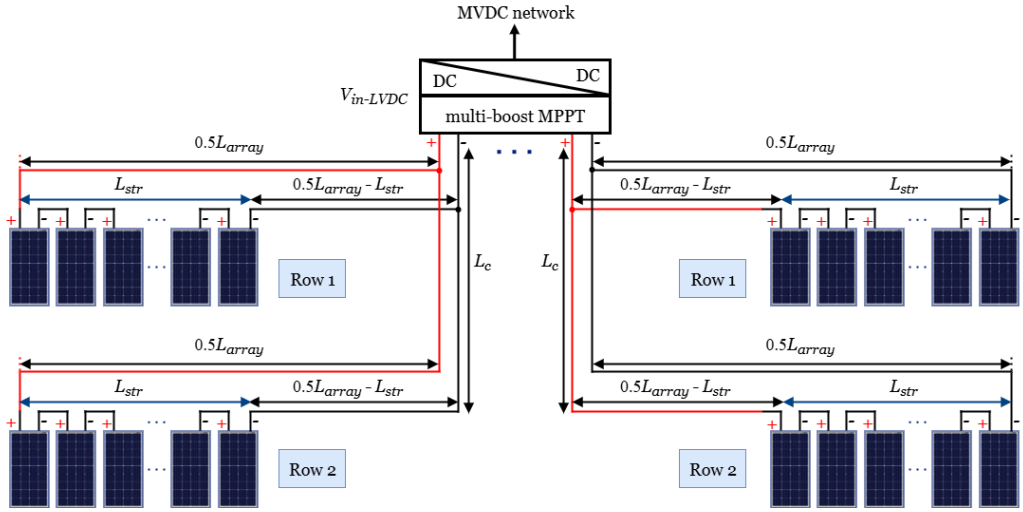


Figure 3. LVDC network configuration of PV string.

The voltage profile is calculated assuming that the PV panels operate at their MPP under standard test conditions. In practical operation, peak shaving may be required due to grid export limits, converter power ratings, or network operating constraints. In such cases, the operating point shifts away from the MPP toward a higher-voltage and lower-current region of the PV characteristic curve. Under these operating conditions, the voltage variation along the cable is lower than that at the MPP due to the reduced current according to Ohm's law. Therefore, cable sizing based on the MPP represents a conservative design criterion and ensures safe operation under all considered operating scenarios. The current and voltage of the PV string circuit can be expressed as

$$I_{str} = I_{MPP}, V_{str} = V_{MPP} \times N_{M_{str}} \tag{8}$$

where I_{str} [A] is the current of the PV string at MPP and V_{str} [V] is the output MPP voltage of the PV string. The voltage rise dV_{str} [V] along the PV string cable is calculated by

$$dV_{str} = \frac{(L_{array} + L_c) \times \rho}{S_{str}} \times I_{str} \tag{9}$$

where S_{str} [mm^2] is the cable cross-sectional area of the string cable to be determined and ρ [$\Omega \cdot$ mm^2/m] is the conductor resistivity. The relative voltage variation dV_{str} [%] with respect to the PV string voltage at MPP is given by

$$\Delta dV_{str} = \frac{|dV_{str}|}{V_{str}} \times 100\% \tag{10}$$

with the LPV string circuit model built in Section 3.1, the PV string cable sizing and results analysis will be discussed in Section 4.

3.2. Modeling of MVDC Collection Network

In this section, the standard MNA formulation adapted to the LPV–MVDC system is first introduced, followed by an analysis of voltage–current coupling effects. Finally, a modified iterative MNA approach is presented.

3.2.1. Standard MNA Formulation

The LPV system interconnected via an MVDC network must first be represented using a standard network formulation consisting of nodes, voltage and current sources, distributed loads, and interconnecting impedance in order to enable a systematic matrix-based formulation. Since the PV arrays interfaced by DC/DC converters are symmetrically distributed along the MVDC network, the voltage profiles on both sides are identical. Therefore, only one side of the system needs to be modeled, as illustrated in Figure 4. The detailed formulation is presented in the following.

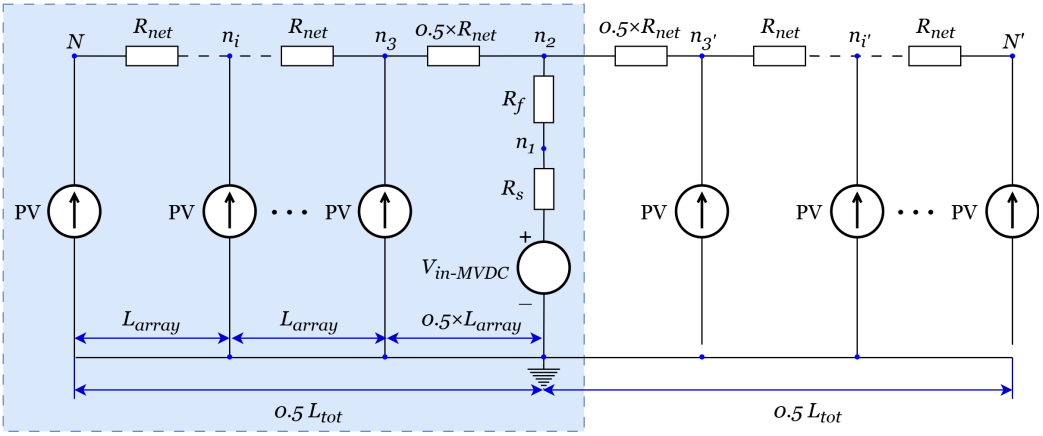


Figure 4. MNA formulation of MVDC collection network for LPV system.

Firstly, the nodes n_1, n_i ..., N are created according to the locations of the DC/DC converters, with $N = N_{DC/DC} + 2$. The MVDC bus is represented as an ideal voltage source $V_{in-MVDC}$ in series with a very small source resistance R_s. The PV arrays, controlled via DC/DC converters, are modeled as current sources. In addition, distributed loads, such as traction or station consumption loads, can be incorporated flexibly if present in the network. Finally, the resistance of the connection cable R_{net-ik} is defined by (11), in which the resistance of the feeder line R_f is given by (12) and the impedance of the network cable R_{net} between adjacent nodes is calculated by (13). It is noted that the cable length is doubled to account for the return path.

$$R_{net-ik} = \begin{cases} R_f & \text{if } i = 1, k = 2 \text{ (feeder line)} \\ 0.5 \times R_{net} & \text{if } i = 2, k = 3 \text{ (half PV array connection cable)} \\ R_{net} & \text{if } i > 2, \text{and } k = i + 1 \text{ (PV array connection cable)} \\ 0 & \text{for others} \end{cases} \tag{11}$$

$$R_f = \rho \times \frac{L_f \times 2}{S_{MV}} \tag{12}$$

$$R_{net} = \rho \times \frac{L_{array} \times 2}{S_{MV}} \tag{13}$$

Based on Figure 4, the general MNA matrix is formulated by

$$\begin{bmatrix} V \\ I \end{bmatrix} = \begin{bmatrix} G & -B \\ B^t & R \end{bmatrix} \begin{bmatrix} J \\ E \end{bmatrix} \tag{14}$$

where G is the conductance matrix of the MVDC collection network, as built by (15), where i and j are the node indices of the row and column of G, respectively. The matrix R is a diagonal matrix in which the element $R_{m,m}$ represents the internal resistance $R_{s,m}$ of the voltage source m, as given in (16), and it is zero elsewhere. The matrix B is the matrix corresponding to Kirchhoff's current equations. As given by (17), the element $B_{i,m}$ is equal to 1 if the voltage source m corresponds to subsystem node i; otherwise, it is equal to 0.

$$G_{i,j} = \begin{cases} -\sum G_{net-ik(i)} & \text{if } j = i \text{ (source node)} \\ G_{net-ik(i)} & \text{if } j = k(i) \text{ (destination nodes)} \\ 0 & \text{for other nodes} \end{cases} \tag{15}$$

$$R_{m,m} = R_{s,m} \quad \text{with the voltage source } m \tag{16}$$

$$B_{i,m} = \begin{cases} 1 & \text{if } m \text{ corresponds to } i \\ 0 & \text{if } m \text{ does not correspond to } i \end{cases} \tag{17}$$

The input vectors J and E represent the known current and voltage sources, respectively. The element J_i is equal to the injected PV current value as defined in (18). The element E_m corresponds to the configured voltage value of the voltage source m, as given in (19). The vectors V and I are the unknown variables, which will be calculated by solving (14). The vector V represents the node voltage with respect to each node along the MVDC collection network. The vector I corresponds to the currents flowing through the branches associated with each voltage source m. There is only one voltage source ($m = 1$) in this case study, thus, $R = R_s$ and $E = V_{in-MVDC}$.

$$J_i = \begin{cases} i_{pv,i} & \text{if } i \text{ is a PV current source} \\ 0 & \text{if } i \text{ is not a PV current source} \end{cases} \tag{18}$$

$$E_m = V_{s,m} \quad \text{with the voltage source } m \tag{19}$$

3.2.2. Nonlinear Voltage–Current Coupling Analysis

In a conventional standard MNA, distributed PV generations are typically modeled as current sources. However, converter-interfaced PV arrays operating under MPPT control behave more closely as constant-power sources. As a result, the injected current at each node depends on the local node voltage. Meanwhile, node voltages vary along the MVDC network due to line impedance and distributed PV current injections. This leads to a voltage–current coupling effect. This coupling introduces nonlinearities that cannot be accurately captured by conventional MNA assuming fixed current injections. To address this issue, a modified MNA framework with an iterative solution scheme is proposed to deal with the resulting nonlinearities. The iterative process updates the voltage-dependent PV current injections at each node until convergence is achieved. It is emphasized that the methodological contribution does not lie in the iterative procedure itself, but in the development of an MNA framework specifically adapted to LPV-MVDC systems. The

proposed iterative approach ensures accurate representation of nonlinear voltage–current coupling while preserving the flexibility and scalability of MNA formulation.

3.2.3. Modified MNA with Iterative Solution

The flowchart of the proposed modified iterative MNA approach is illustrated in Figure 5. The iterative scheme continuously updates the PV current injections according to the local node voltages, thereby improving the accuracy of power loss and voltage profile calculations. The iterative solution procedure is summarized as follows:

(0) Initialize the essential parameters illustrated in Figure 4.

(1) Build the matrices G, R, B, J, and E according to (15)–(19).

(2) Initialize all node voltages using the nominal voltage $v_i^{(0)} = V_{in-MVDC}$. During the first iteration, each PV source is modeled as a constant current source, where the injected current is initialized as

$$i_{PV,i}^{(0)} = \frac{P_{array}}{V_{in-MVDC}} \tag{20}$$

Considering DC/DC conversion efficiency, the injected PV power at MPP is given by

$$P_{array} = P_{mod} \times N_{M_{\text{array}}} \times 2 \times \eta \tag{21}$$

where η denotes the converter efficiency, typically ranging from 0.95 to 0.99.

(3) Solve the MNA matrix using (14) to obtain the updated voltage vector, denoted by $\widetilde{V}^{(k)}$, together with the corresponding branch currents.

(4) Apply a relaxation update to improve numerical stability and suppress oscillatory behavior commonly observed in constant-power systems. The relaxed voltage update is expressed as

$$V^{(k)} = \alpha \widetilde{V}^{(k)} + (1-\alpha) V^{(k-1)} \tag{22}$$

where $\widetilde{V}^{(k)}$ is the voltage vector obtained from the MNA solution at iteration k, $V^{(k-1)}$ is the voltage vector from the previous iteration, and α is the relaxation coefficient. In practice, stable convergence is generally achieved for $0.3 \leq \alpha \leq 0.7$.

(5) The injected current is dynamically updated by (23), where $v_i^{(k)}$ is the updated voltage for node i at iteration k.

$$i_{PV,i}^{(k)} = \frac{P_{array}}{v_i^{(k)}} \tag{23}$$

(6) Check the convergence criterion:

$$\max \left| V^{(k)} - V^{(k-1)} \right| < \epsilon \tag{24}$$

where ϵ is the convergence tolerance, typically selected within the range 10^{-3} to 10^{-6}.

(7) If the convergence criterion is not satisfied, repeat steps (3)–(6) until convergence is achieved.

(8) If the convergence criterion is satisfied, compute final quantities including voltage profiles, branch currents, power losses, etc.

The iterative current calculation approach improves calculation precision compared with the fixed-current assumption, as PV currents are updated with local node voltages, which will be verified in Section 4.

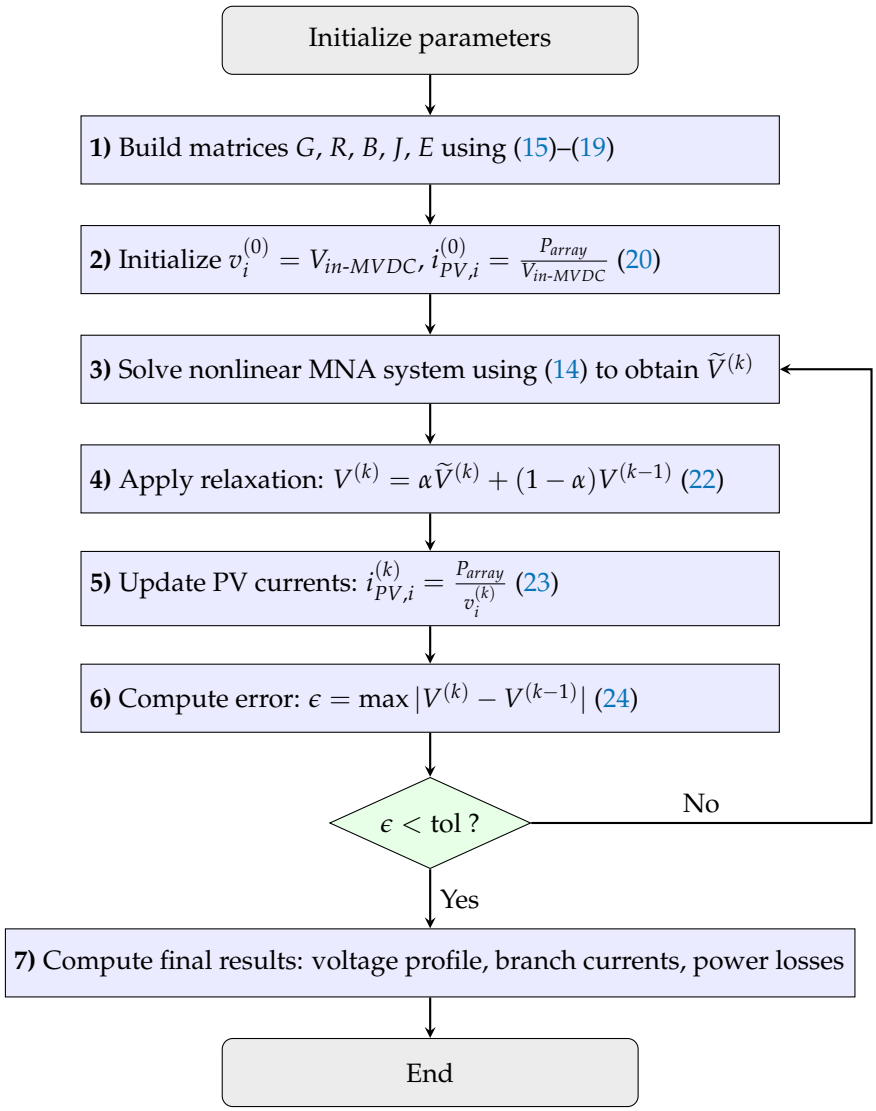


Figure 5. Flowchart of iterative nonlinear MNA solution applied to LPV MVDC collection network.

4. Results Analysis

The extensive physical layout of the LPV plant, combined with the significant distance between the LPV installations and the nearest AC grid substation, poses challenges for the distribution network [8]. Firstly, the PV strings are extended over a certain distance before being connected with boost converters for MPPT. The voltage increase for the most distant PV module should be maintained within the limit. Secondly, the MVDC network design should ensure acceptable voltage variations between the most distant LV-MV DC/DC converter and the MVDC bus. The LVDC and MVDC cables must be appropriately selected to comply with voltage variation constraints defined in Section 4.1. It is worth mentioning that design standards must be adapted to practical constraints in a real implementation project.

4.1. LPV Collection Network Design Principle

As no specific standards currently exist for the design of LPV systems, two main references are considered to establish the design principles: the PV installation guidelines published by UTE (Union Technique de l'Électricité) [25] and the published results of the OPHELIA project [8]. In particular, the following design principles are considered:

- The voltage variation along the PV string in the LVDC part shall not exceed 3% at STC conditions, a limit of 1% is recommended.
- The voltage variation in the MVDC collection network shall not exceed 5% at STC conditions, a limit of 3% is recommended.
- The voltage variation dV_{AC} between the point of delivery and the AC terminals of the inverter shall not exceed 3% at rated power, and a limit of 1% is recommended. The resistance of the connection between the point of delivery and the AC terminals of the inverter shall be $\leq$0.5 Ω. The DC/AC converter is assumed to be located very close to the power transformer, resulting in negligible voltage variations on the AC side. Therefore, this work focuses on the LVDC and MVDC network and their cable sizing.

4.2. Sizing Results of LVDC PV String Cable

PV strings are symmetrically arranged as shown in Figure 3. As a result, the voltage profiles along the PV string exhibit symmetric behavior, as illustrated in Figure 6. The voltage increases along the connection cable and reaches its maximum at the end of the PV string. The maximum relative voltage variations for different cable cross-sections are presented in Figure 7. It can be observed that the voltage variations remain less than 1% for conductor cross-sections ranging from 6 mm^2 to 50 mm^2. Based on these results, a standard copper cable with a cross-section of 6 mm^2 is selected for the string-level connections, which ensures that voltage variations remain within the 1% constraint.

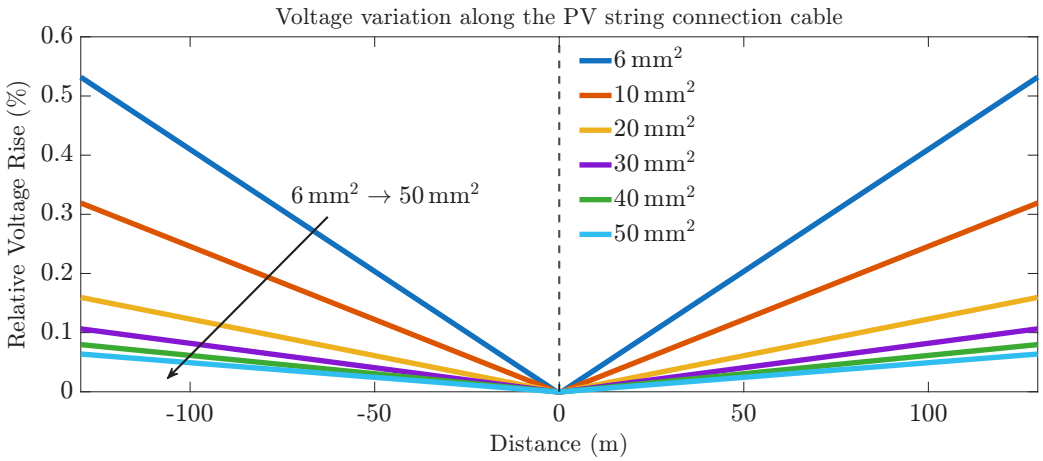


Figure 6. Relative voltage increase along the PV string connection cable.

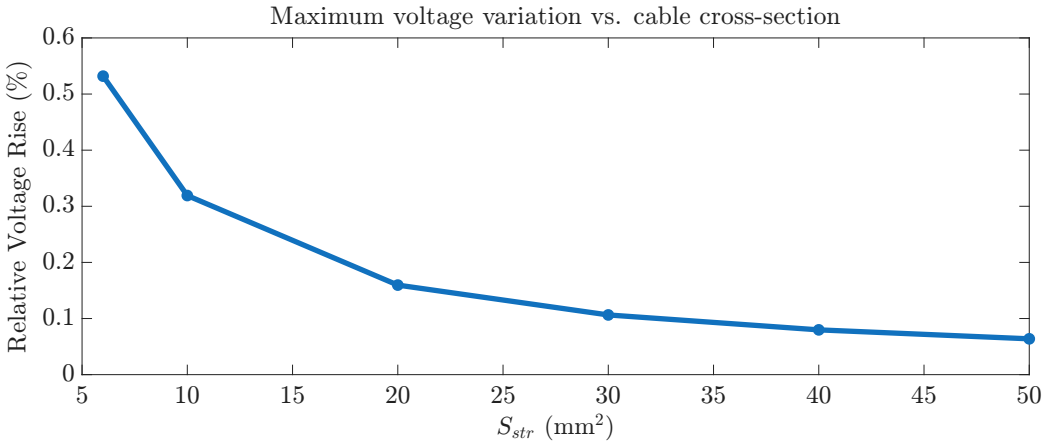


Figure 7. Maximum voltage variations at the most distant point under different cross sections.

4.3. Sizing Results of MVDC Connection Cable

Firstly, the effectiveness of the proposed iterative MNA approach is verified through comparison with the conventional fixed-current MNA formulation. Figure 8 compares the absolute and relative errors between the two methods for different conductor cross-sections. As shown in Figure 8a, the absolute error increases with distance along the MVDC feeder due to the progressive accumulation of voltage rise and the resulting deviations in PV current injections. A similar trend is observed for the relative error in Figure 8b. The largest difference occurs for the 50 mm^2 conductor, reaching an absolute error of approximately 54 V and a relative error of 0.26% at the feeder end. Such errors introduced by the conventional MNA formulation can lead to inaccuracies in network sizing and component dimensioning. Furthermore, increasing the conductor cross-sectional area reduces both the absolute and relative errors. This behavior is attributed to the lower line resistance and the resulting reduction in voltage variations along the feeder. These results demonstrate that the impact of nonlinear voltage–current coupling becomes increasingly significant in long-distance feeders with high line impedance. The results also confirm the necessity and effectiveness of the proposed iterative MNA formulation for accurately modeling LPV systems interconnected through MVDC networks.

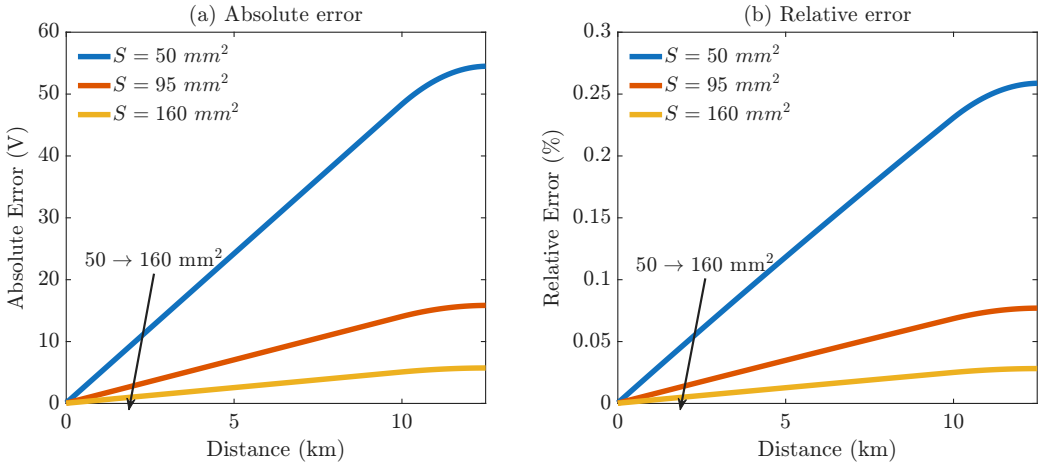


Figure 8. Comparison between fixed-current MNA and proposed iterative MNA.

Figure 9 shows the relative voltage rise referenced to the MVDC bus voltage as a function of distance from the MVDC bus to the end of the LPV power plant. Different cable cross-sectional areas are investigated under both the fixed-current MNA and the iterative MNA formulation. Firstly, the linear transmission zone is from the MVDC bus to the end of the feeder line, with L_f assumed to be 10 km. The voltage variation increases linearly with distance along the feeder. A nonlinear deviation appears in the PV injection zone from 10 km to the most distant PV injection point. Secondly, the iterative solution yields slightly lower voltage rise than the fixed-current assumption. This is because a higher local node voltage reduces the injected current for the same PV power, which in turn decreases the voltage rise. These results also highlight the importance of considering the nonlinear behavior of PV generation for accurate assessment of network performance. Finally, cables with greater cross-sectional areas provide better voltage stability over distance compared to smaller cables, at the expense of higher capital investment.

A systematic sensitivity analysis of main parameters is provided in Figure 10. Figure 10a,b compare copper and aluminum conductors under the same voltage level, while Figure 10a,c compare voltage variations under different voltage levels using a copper conductor. The sensitivity analysis shows that conductor material, cross-sectional area, and system voltage level influence the voltage profiles along the MVDC network. The

conductor material determines the line resistivity, where copper provides lower resistance than aluminum, resulting in reduced voltage rise. The cross-sectional area directly affects the cable resistance, with larger sections improving voltage regulation by decreasing ohmic losses. In addition, the system voltage level affects the current magnitude for a given power transfer. Higher voltage operation reduces line currents and decreases voltage variations along the feeder. Overall, these parameters jointly determine the voltage profile and are critical for ensuring compliance with MVDC design constraints.

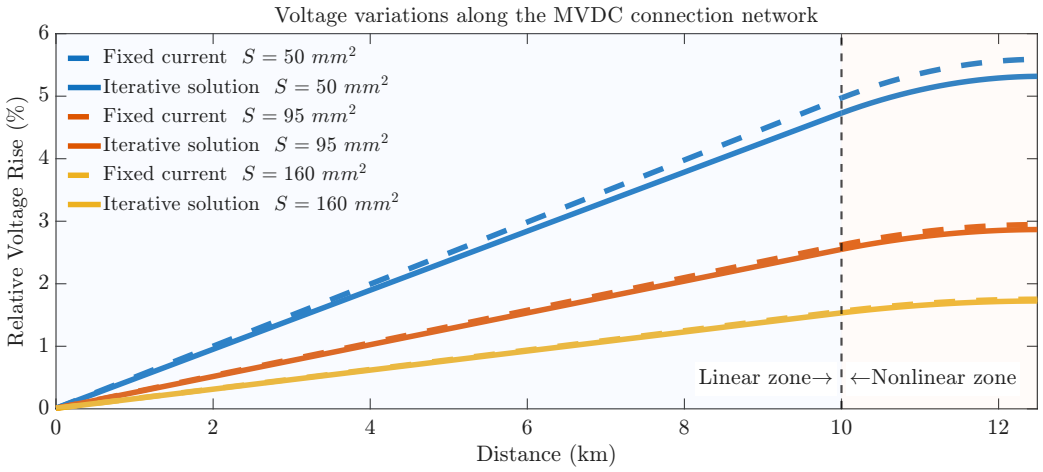


Figure 9. Relative voltage increase along the MVDC connection cable.

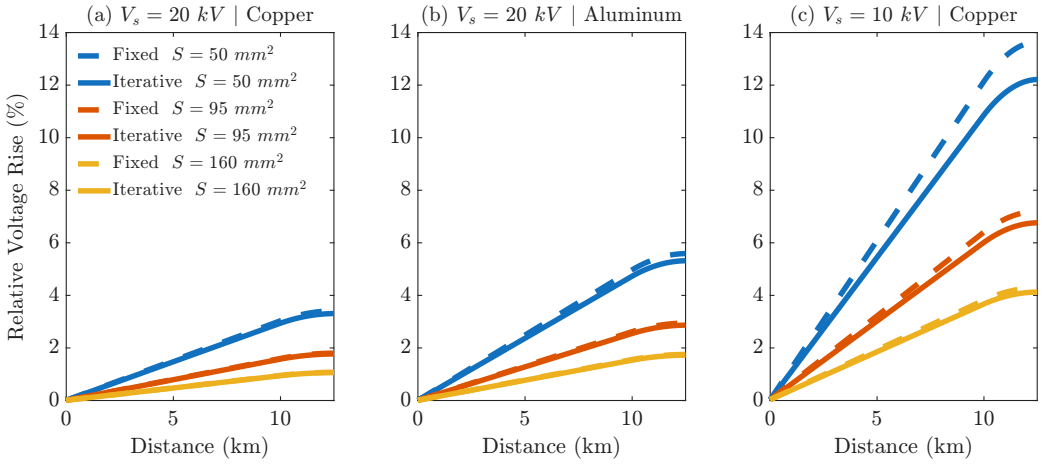


Figure 10. Comparative results: (**a**) Reference case, (**b**) different conductor materials comparison, (**c**) different voltage levels comparison.

According to the design constraints in Section 4.1, the relative voltage variation between the MVDC substation and the most distant PV array injection point must be less than 5%, with a recommended limit of 3%. From the results, a copper conductor with a cross-sectional area of 95 mm^2 is selected, and a 20 kV voltage level is identified for the MVDC distribution network.

5. Discussion

5.1. Study Limitations

- Overall, most medium-voltage and high-power DC/DC converter technologies remain at the research or prototype stage, with no commercially available products currently on the market. As a result, the layout design and sizing results presented in this work should be regarded as a theoretical assessment of LPV size and converter capacity.

Nevertheless, the proposed layout design and modeling methodology is flexible to be adapted to the technical specifications of converters used in future projects.

- Furthermore, additional validation using detailed simulation platforms, DC distribution test benchmarks, or experimental demonstrators would be beneficial to fully assess the proposed methodology. However, such validation remains limited due to the absence of a commercially available MVDC converter designed for long-distance, high-power LPV applications. Therefore, a comprehensive validation using advanced simulation tools and experimental setups remains important work in the future.
- In addition, critical technical specifications and cost data remain confidential, preventing a precise economic assessment of LPV installations at this stage. Consequently, a comprehensive economic assessment is beyond the scope of this study and is left for future work.

Nevertheless, to enhance the practical relevance of the proposed LPV–MVDC power system, a brief discussion of practical challenges and expected economic impacts is provided in the following subsections.

5.2. Practical Challenges

From a practical perspective, several challenges remain for the implementation of the proposed LPV system based on an MVDC architecture. These challenges include:

- LPV systems can extend over several kilometers along highways or railways, requiring coordination with existing infrastructure, land-use constraints, safety regulations, and maintenance access. Installation and operation may be affected by corridor-specific requirements and permissions from infrastructure operators.
- An LPV-MVDC system requires medium-voltage and high-power DC/DC converter stations distributed over long-distance corridors. These converters potentially increase system complexity, installation requirements, maintenance needs, and capital investment compared with conventional centralized PV systems.
- DC fault currents rise rapidly and lack natural current zero-crossings, making fault detection more challenging than in AC systems. Reliable MVDC protection strategies and suitable DC circuit breakers are still evolving technologies and may increase implementation costs in the short term.
- Finally, MVDC distribution systems are not yet as mature as conventional AC distribution networks. Standards, protection practices, and grid-connection requirements for large-scale MVDC-based LPV installations are still under development.

5.3. Techno-Economic Analysis

A simplified engineering-oriented techno-economic discussion is provided to highlight key cost-driving parameters of the proposed LPV-MVDC architecture.

- From a converter perspective, the proposed design results in two feasible configurations: (i) 40 DC/DC converter stations rated at 100 kW each, and (ii) 20 converter stations rated at 200 kW each. The first configuration increases the number of power electronic units, which typically leads to higher installation cost, control complexity, and maintenance effort. However, it benefits from improved MPPT efficiency and reduced mismatch losses along the corridor. In contrast, the second configuration reduces the number of converter stations, thereby lowering capital costs. But it requires higher individual converter ratings and potentially increases mismatch losses.
- Cable sizing also has a direct economic impact. At LVDC level, a 6 mm^2 copper conductor is sufficient to meet the voltage drop constraint, minimizing material cost while maintaining compliance. At MVDC level, a 95 mm^2 copper conductor is required to satisfy the 5% voltage variation limit over long distances. If aluminum conductors

are considered as an alternative, the initial material cost could be reduced. However, this comes at the expense of higher resistivity, requiring larger cross-sectional areas and leading to increased conduction losses and potentially higher life-cycle cost.

- Regarding power losses, the dominant losses originate from ohmic losses along the cables. Increasing the conductor cross-sectional areas or a higher DC voltage level can reduce these losses. However, both measures lead to higher capital investment costs. This results in a trade-off between energy efficiency and investment cost.

Overall, the design reveals a three-way trade-off between (i) converter quantity and rating power, (ii) conductor material and sizing, and (iii) resistive power losses. These relationships provide practical design guidelines for early-stage planning of LPV-MVDC systems. The detailed economic impacts, optimization incorporating cost functions and time-dependent energy yield, are left for future work.

6. Conclusions

This paper presents a systematic design and modeling methodology for LPV-MVDC system integrated along railway and highway corridors. The main methodological contribution is the development of an iterative MNA framework tailored to LPV–MVDC systems. The nonlinear voltage–current coupling effect becomes significant in long-distance feeders with high line impedance. The comparative results with conventional MNA demonstrate the effectiveness of the proposed iterative MNA method in accurately capturing these nonlinear effects. A 5 km railway corridor with vertical two-row PV installations is considered as a case study to illustrate the proposed design and modeling methodology. Some key quantitative results obtained from the case study are summarized as follows:

- Firstly, both electrical safety margins and land-use constraints are considered in the LPV layout design. A string configuration of 18 series-connected PV modules ensures an adequate safety margin under low-temperature operating conditions. Each array consists of six PV strings, corresponding to a total of 108 PV modules. The 5 km LPV power plant achieves a total installed capacity of 3.4 MW at the MPP.
- Based on the proposed design methodology, two feasible configurations are explored: (i) 40 DC/DC converter stations rated at 100 kW each, and (ii) 20 converter stations rated at 200 kW each. The first configuration increases the number of power electronic units, leading to higher installation costs, system complexity, and maintenance requirements. However, it offers improved MPPT performance and smaller mismatch losses along the corridor. In contrast, the second configuration reduces the number of converter stations. However, it requires higher converter ratings and may increase mismatch losses between PV modules.
- Regarding the electrical architecture design, DC/DC converter stations with multi-input MPPT channels are chosen to mitigate mismatch effects along the corridor. The sizing results focus on the first layout configuration. Cable analysis shows that 6 mm^2 copper conductors satisfy the 1% voltage drop constraint at LVDC level. A 95 mm^2 copper conductor operating at 20 kV ensures that voltage variations remain below 3% for the MVDC network, complying with voltage variation limits.

Finally, practical deployment of an LPV-MVDC system still faces challenges related to the availability of commercial MVDC converters, DC protection systems, and maintenance requirements. Despite these challenges, the LPV-MVDC concept offers long-term potential by enabling efficient power transmission along linear infrastructures while exploiting underused railway and roadside corridors. As most high-power DC/DC converter technologies are still at the prototype stage, the presented results should be interpreted as a theoretical design framework. It provides a scalable methodology rather than finalized industrial specifications. A detailed techno-economic assessment considering capital

expenditure, operational costs, energy yield, and life-cycle costs will be investigated in future work. In addition, comprehensive validation using advanced simulation tools and experimental setups remains an important direction for future research.

Author Contributions: B.G. wrote the article, conducted the literature review, prepared all figures, developed the modified MNA method with iterative solution, and performed the simulations and results analysis. M.A. contributed to the PV string and array layout design, supported the development of MNA modeling, and assisted in manuscript preparation. D.B. provided guidance on PV design principles as well as PV string and array layout configuration. J.P. provided technical advice on the integration of LPV systems into railway infrastructures. B.B. provided proofreading and correction feedback. All authors have read and agreed to the published version of the manuscript.

Funding: This work is funded by project LINPV4Railway—LINear PV for Electrical Railway Applications, funded by the Innosuisse Chèque d'Innovation program under grant NO. 75314.1 INNO-EE.

Data Availability Statement: The original contributions presented in this study are included in the article. Further inquiries can be directed to the corresponding author.

Acknowledgments: The authors acknowledge the use of generative artificial intelligence tools for language refinement and editing support during the preparation of this manuscript. The authors remain fully responsible for the content, analyses, and conclusions presented in this work.

Conflicts of Interest: The authors declare no conflicts of interest.

Nomenclature

Abbreviations

AC	Alternating Current
DC	Direct Current
DC/DC	Direct Current to Direct Current Converter
DC-SST	DC Solid-State Transformer
HVDC	High-Voltage Direct Current
LPV	Linear Photovoltaic
LVDC	Low-Voltage Direct Current
MMC	Modular Multilevel Converter
MNA	Modified Nodal Analysis
MPPT	Maximum Power Point Tracking
MVAC	Medium-Voltage Alternating Current
MVDC	Medium-Voltage Direct Current
PV	Photovoltaic
RES	Renewable Energy Sources
SiC	Silicon Carbide
STC	Standard Test Condition
VSC	Voltage Source Converter

Vectors and Matrices

B	Incidence matrix of voltage sources	[-]
E	Voltage source vector	[V]
G	Conductance matrix	[S]
I	Branch current vector	[A]
J	Current injection vector	[A]
R	Source resistance matrix	[Ω]
V	Node voltage vector	[V]
$\widetilde{V}^{(k)}$	Updated voltage vector at iteration k	[V]
$V^{(k)}$	Voltage vector at iteration k	[V]

Latin Symbols

dV_{AC}	AC-side voltage variation	[V]

dV_{str}	Voltage variation along PV string cable	[V]
I_{MPP}	Current at maximum power point	[A]
$i_{PV,i}$	PV current injected at node i	[A]
$i_{PV,i}^{(k)}$	PV current at node i at iteration k	[A]
I_{sc}	Short-circuit current of PV module	[A]
I_{str}	PV string current	[A]
L_{array}	Length of PV array	[m]
L_c	Crossing cable length of roads or railway track	[m]
L_D	Distance leaving for converter installations	[m]
L_d	Distance between PV modules	[m]
L_f	Feeder line length	[m]
L_{mod}	Width of PV module	[m]
L_{str}	Length of PV string	[m]
L_{tot}	Total length of LPV power plant	[m]
N_{array}	Number of arrays	[-]
$N_{DC/DC}$	Number of DC/DC converters	[-]
$N_{M_{array}}$	Number of modules per PV array	[-]
$N_{M_{str}}$	Number of modules per PV string	[-]
N_{str}	Number of strings per PV array	[-]
P_{array}	PV array power	[W]
P_{mod}	PV module power	[W]
R_f	Feeder resistance	[Ω]
R_{net}	Network resistance between two nodes	[Ω]
R_{net-ik}	Resistance between nodes i, k	[Ω]
R_s	Source internal resistance	[Ω]
S_{MV}	MVDC cable cross-section	[mm^2]
S_{str}	String cable cross-section	[mm^2]
T	Temperature	[°C]
v_i	Node voltage at node i	[V]
$v_i^{(k)}$	Node voltage at node i at iteration k	[V]
$V_{in-LVDC}$	LVDC bus voltage	[V]
$V_{in-MVDC}$	MVDC bus voltage	[V]
V_{MPP}	PV module voltage at MPP	[V]
V_{oc}	Open-circuit voltage of PV module	[V]
V_{str}	String voltage	[V]
ΔdV_{str}	Relative voltage drop along PV string	[%]
Greek Symbols		
α	Relaxation factor used in MNA iteration	[-]
$\alpha_{I_{sc}}$	Temp. coefficient of short-circuit current	[%/°C]
$\beta_{V_{oc}}$	Temp. coefficient of open-circuit voltage	[%/°C]
ϵ	Convergence tolerance	[-]
η	Converter efficiency	[-]
ρ	Electrical resistivity	[Ω· mm ^{2}/m]

References

1. Walch, A.; Rüdisüli, M. Energy Strategy 2050: The Potential of Millions of Swiss Rooftops. 2022. Available online: https://www.sciena.ch/research/energy-strategy-2050-the-potential-of-millions-of-swiss-rooftops.html (accessed on 28 June 2025).
2. Pouget, J.; Guo, B.; Meier, T.; Scuderi, J.; Boisset, F. Vers un smart grid ferroviaire. Un microgrid ferroviaire au service de la transition énergétique. *Bulletin.ch (Electrosuisse et AES)* **2024**, *6*, 2–7.
3. Niccolai, A.; Cirimele, V.; Franceschini, D.; Apicella, V.; Carambia, B.; Leva, S. Highway PV capacity potential: A GIS-Driven approach for assessment and prioritization. *Sustain. Energy Technol. Assess.* **2025**, *81*, 104384. [CrossRef]
4. Asanov, I.M.; Loktionov, E.Y. Possible benefits from PV modules integration in railroad linear structures. *Renew. Energy Focus* **2018**, *25*, 1–3. [CrossRef]

5. Wei, F.; Li, Y.; Fan, Y. Arrangement optimization based on shadow adaptation for strip PV arrays along electrified railways corridors. *Energy Convers. Manag.* **2025**, *336*, 119753. [CrossRef]
6. Kakoulaki, G.; Szabo, S.; Fahl F, F.; Taylor, N.; Gracia-Amillo, A.; Kenny, R.; Ulpiani, G.; Chatzipanagi, A.; Gkoumas, K.; Jäger-Waldau, A. European transport infrastructure as a solar photovoltaic energy hub. *Renew. Sustain. Energy Rev.* **2024**, *196*, 114344. [CrossRef]
7. Cornaggia, L.; Girard, R.; Despouys, O.; Clemot, H.; Andrianesis, P. Comparison of Losses and Costs between AC and MVDC Connections for New DC Resources. In *Proceedings of the 2023 IEEE PES Innovative Smart Grid Technologies Europe (ISGT EUROPE)*; IEEE: Piscataway, NJ, USA, 2023; pp. 1–5.
8. Dworakowski, P.; Marache, S.; Lamard, E.; Ramondou, C. Linear PV power plant based on MVDC collection network. In Proceedings of the CIGRE Session, Paris, France, 25–30 August 2024.
9. Long, C.; Wu, J.; Smith, K.; Moon, A.; Bryans, R.; Yu, J. MVDC link in a 33 kV distribution network. *CIRED* **2017**, *2017*, 1308–1312. [CrossRef]
10. Reed, G.F.; Grainger, B.M.; Sparacino, A.R.; Mao, Z.H. Ship to Grid: Medium-Voltage DC Concepts in Theory and Practice. *IEEE Power Energy Mag.* **2012**, *10*, 70–79. [CrossRef]
11. Reed, G.F.; Grainger, B.M.; Sparacino, A.R.; Kerestes, R.J.; Korytowski, M.J. Advancements in medium voltage DC architecture development with applications for powering electric vehicle charging stations. In Proceedings of the 2012 IEEE Energytech, Cleveland, OH, USA, 29–31 May 2012; pp. 1–8. [CrossRef]
12. Hassan, S.J.U.; Mehdi, A.; Haider, Z.; Song, J.S.; Abraham, A.D.; Shin, G.S.; Kim, C.H. Towards medium voltage hybrid AC/DC distribution Systems: Architectural Topologies, planning and operation. *Int. J. Electr. Power Energy Syst.* **2024**, *159*, 110003. [CrossRef]
13. Eissa, M. Medium-Voltage Direct Current Concept, Modeling, Operation, Control, Protection, and Management—An Extensive Article Review. In *Medium Voltage Direct Current Grid*; Academic Press: Cambridge, MA, USA, 2019; pp. 1–41.
14. Coffey, S.; Timmers, V.; Li, R.; Wu, G.; Egea-Álvarez, A. Review of MVDC Applications, Technologies, and Future Prospects. *Energies* **2021**, *14*, 8294. [CrossRef]
15. Le Métayer, P.; Paez, J.; Touré, S.; Buttay, C.; Dujic, D.; Lamard, E.; Dworakowski, P. Break-even distance for MVDC electricity networks according to power loss criteria. In *Proceedings of the 2021 23rd European Conference on Power Electronics and Applications (EPE'21 ECCE Europe)*; IEEE: Piscataway, NJ, USA, 2021; pp. 1–9.
16. Siddique, H.A.B.; Ali, S.M.; De Doncker, R.W. DC collector grid configurations for large photovoltaic parks. In *Proceedings of the 2013 15th European Conference on Power Electronics and Applications (EPE)*; IEEE: Piscataway, NJ, USA, 2013; pp. 1–10.
17. Gil, M.D.P.; Domínguez-García, J.L.; Díaz-González, F.; Aragüés-Peñalba, M.; Gomis-Bellmunt, O. Feasibility analysis of offshore wind power plants with DC collection grid. *Renew. Energy* **2015**, *78*, 467–477. [CrossRef]
18. Projet OPHELIA: CNR et Ses Partenaires Innovent Avec le Lancement d'un Démonstrateur d'Ombrières Solaires sur la ViaRhôna. 2025. Available online: https://www.cnr.tm.fr/actualites/projet-ophelia-cnr-et-ses-partenaires-innovent-avec-le-lancement-dun-demonstrateur-dombrieres-solaires-sur-la-viarhona/ (accessed on 20 June 2025).
19. Métayer, P.L.; Loeuillet, Q.; Wallart, F.; Buttay, C.; Dujic, D.; Dworakowski, P. Phase-Shifted Full Bridge DC–DC Converter for Photovoltaic MVDC Power Collection Networks. *IEEE Access* **2023**, *11*, 19039–19048. [CrossRef]
20. Nielsen, M. *Control of Medium Voltage Power Converters Enabled by 10 kV SiC MOSFETs*; Aalborg University Open Publishing: Aalborg East, Denmark, 2025. [CrossRef]
21. Rothmund, D.; Ortiz, G.; Guillod, T.; Kolar, J.W. 10kV SiC-based isolated DC-DC converter for medium voltage-connected Solid-State Transformers. In Proceedings of the 2015 IEEE Applied Power Electronics Conference and Exposition (APEC), Charlotte, NC, USA, 15–19 March 2015; pp. 1096–1103. [CrossRef]
22. RCT Systems. *SST Spec Sheet: 1.8 MW Scalable Solid-State Transformer System*; Specification Sheet; RCT Systems: Baltimore, MD, USA, 2024. Available online: https://www.rct-systems.com/wp-content/uploads/2024/05/03-RCT-Spec-Sheets-SST.pdf (accessed on 24 November 2025).
23. Nami, A.; Liang, J.; Dijkhuizen, F.; Demetriades, G.D. Modular Multilevel Converters for HVDC Applications: Review on Converter Cells and Functionalities. *IEEE Trans. Power Electron.* **2015**, *30*, 18–36. [CrossRef]
24. Sun, P.; Pinthurat, W.; Li, G.; Khalid, M.; Town, G.E.; Konstantinou, G. Adaptive Droop Control in VSC-Based MT-MVDC Distribution Systems Considering ESS Participation. *IEEE Trans. Energy Convers.* **2025**, *40*, 761–772. [CrossRef]
25. Union Technique de l'Électricité (UTE). *Installations électriques à Basse Tension: Guide Pratique—Installations Photovoltaïques Raccordées au Réseau Public de Distribution (UTE C 15-712-1)*; Technical Report; UTE: Puteaux, France, 2010.
26. Mayet, C.; Arboleya, P.; Bouscayrol, A.; Mohamed, B.; Delarue, P.; El-Sayed, I. Non-linear switched model for accurate voltage estimation and power flow analysis of DC railway systems. *IET Electr. Syst. Transp.* **2020**, *10*, 425–435.
27. Guo, B.; Pouget, J.; Bossoney, L.; Carpita, M.; Meier, T.; Maye, J.P. Catenary overvoltage stabilization of DC railway electrical system by integrating EV charging stations. In Proceedings of the 2022 20th International Conference on Harmonics & Quality of Power (ICHQP), Naples, Italy, 29 May–1 June 2022; pp. 1–6. [CrossRef]

28. Montoya, O.D.; Garrido, V.M.; Gil-González, W.; Grisales-Noreña, L.F. Power Flow Analysis in DC Grids: Two Alternative Numerical Methods. *IEEE Trans. Circuits Syst. II Express Briefs* **2019**, *66*, 1865–1869. [CrossRef]
29. Montoya, O.D.; Grisales-Noreña, L.; González-Montoya, D.; Ramos-Paja, C.; Garces, A. Linear power flow formulation for low-voltage DC power grids. *Electr. Power Syst. Res.* **2018**, *163*, 375–381. [CrossRef]
30. Meyer Burger Technology AG. *Black Module Datasheet*; Technical Report; Meyer Burger Technology AG: Gwatt, Switzerland, 2023. Available online: https://krannich-solar.com/fileadmin/user_upload/GR/Products/Modules/Meyer_Burger/MB-375HJT-M_120_Full_Black__Mono_.pdf (accessed on 8 June 2025).
31. Hashem, A.M.A.L. Thermal Energy Storage for Building-Integrated Photovoltaic Components. Ph.D. Thesis, University of Strathclyde, Glasgow, Scotland, 2011.
32. Yousri, D.; Allam, D.; Eteiba, M.B. Optimal photovoltaic array reconfiguration for alleviating the partial shading influence based on a modified harris hawks optimizer. *Energy Convers. Manag.* **2020**, *206*, 112470. [CrossRef]
33. Shams El-Dein, M.Z.; Kazerani, M.; Salama, M.M.A. Optimal Photovoltaic Array Reconfiguration to Reduce Partial Shading Losses. *IEEE Trans. Sustain. Energy* **2013**, *4*, 145–153. [CrossRef]

Disclaimer/Publisher's Note: The statements, opinions and data contained in all publications are solely those of the individual author(s) and contributor(s) and not of MDPI and/or the editor(s). MDPI and/or the editor(s) disclaim responsibility for any injury to people or property resulting from any ideas, methods, instructions or products referred to in the content.